Noname manuscript No.
(will be inserted by the editor)

Mechanical Properties of Cellulose Nanofibril Films: Effects of Crystallinity and its Modification by Treatment with Liquid Anhydrous Ammonia

Vegar Ottesen · Per Tomas Larsson · Gary Chinga-Carrasco · Kristin Syverud · Øyvind Weiby Gregersen

Received: date / Accepted: date

Abstract The influence of cellulose crystallinity on mechanical properties of cellulose nano-fibrils (CNF) was investigated. Degree of crystallinity (DoC) was modified using liquid anhydrous ammonia. Such treatment changes crystal allomorph from cellulose I to cellulose III, a change which was reversed by subsequent boiling in water. DoC was measured using solid state nuclear magnetic resonance (NMR). Crystalline index (CI) was also measured using wide angle x-ray scattering (WAXS). Cotton linters were used as the raw material. The cotton linter was ammonia treated prior to fibrillation. Reduced DoC is seen to associate with an increased yield point and decreased Young modulus. Young modulus is here defined as the maximal slope of the stress-strain curves. The association between DoC and Young modulus or DoC and yield point are both statistically significant. We cannot conclude there has been an effect on strainability. While mechanical properties were affected, we found no indication that ammonia treatment affected degree of fibrillation. CNF was also studied in air and liquid using atomic force microscopy (AFM). Swelling of the nanofibers was observed, with a mean diameter increase of 48.9%.

V. Ottesen
Department of Chemical Engineering, NTNU, Trondheim, Norway
E-mail: vegar.ottesen@ntnu.no

P. T. Larsson
RISE Bioeconomy, Stockholm, Sweden
and KTH Royal Institute of Technology, Stockholm, Sweden

G. Chinga-Carrasco
RISE PFI, Trondheim, Norway

K. Syverud
RISE PFI, Trondheim, Norway
and Department of Chemical Engineering, NTNU Trondheim, Norway

Ø. W. Gregersen
Faculty of Natural Sciences, NTNU, Trondheim, Norway
E-mail: oyvind.w.gregersen@ntnu.no

1 Introduction

Society is increasingly valuing "green" materials and products. Non-renewable materials like non-biodegradable plastics and plastics from fossil feedstocks like oil are under increasing pressure. Biodegradable, renewable alternatives are actively sought by consumers and policy makers alike - especially for short service life applications such as packaging and disposables used for food preparation and consumption (Brodin et al. 2017).

For packaging applications, cellulose nano-fibrils (CNF) may present one such green alternative. Films from CNF may be transparent (Nogi et al. 2009), have excellent gas barrier properties (Syverud and Stenius 2008; Aulin et al. 2010; Fukuzumi et al. 2009), and high tensile strength (Henriksson et al. 2008). One of the properties not conducive to the adoption of this "green" material is the limited ductility of CNF based films as compared to currently employed plastic materials. CNF films are typically brittle - they are stiff and exhibit low extensibility as compared to many plastic alternatives (Rodionova et al. 2012). This brittleness prevents folding and shaping of the CNF based product, limiting applicability and appeal.

Controlling the stiffness, extensibility of CNF could open new markets for the material and allow for greater flexibility in terms of applications. Various strategies have previously been employed. Examples include addition of plasticizers (Myllytie et al. 2010; Minelli et al. 2010; Kumar et al. 2016), embedding nanofibrils in a more ductile matrix material (Nishino et al. 2004), or chemical or structural modification of the nanofibril surface (P. A. Larsson, Berglund, et al. 2014; Codou et al. 2015; P. A. Larsson and Wågberg 2016). Both the use of all-cellulose composites (Nishino et al. 2004), and amorphization of fibril surfaces (P. A. Larsson, Berglund, et al. 2014; P. A. Larsson and Wågberg 2016) make use of the link between flexibility and crystallinity of a material. In the current work, we used submersion in anhydrous ammonia to reduce the general crystallinity of the cellulose, while minimally affecting the degree of polymerization or the surface chemistry. Ammonia treatment is associated with strong reduction in crystallinity and a change in crystal allomorph. In order to preserve the crystal allomorph, the ammonia submersion was followed by a hydrothermal treatment, reverting it to cellulose I. Cotton linters were used for their high purity and high degree of crystallinity.

2 Materials and Methods

The current work describes CNF prepared by homogenization of cotton linters. Samples are referred to as CNF-n where n is a number indicating the number of ammonia treatments the sample has undergone, either 0, 1 or 3.

Most numerical and statistical analysis was performed using the statistical software "R" v. 3.5.0 (R Core Team 2015). Software developed at Innventia AB, Sweden was used for NMR data, as indicated. Plots were generated using ggplot2 v. 3.0.0 (Ginestet 2011) or Ti*k*Z (Figures 12, 5, 8, 1).

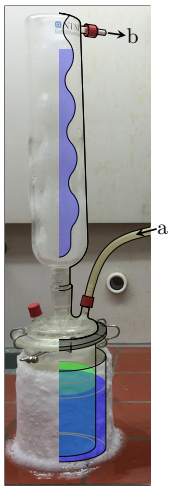

Fig. 1 Ammonia treatment. Material to be treated was put in a closed reaction vessel, which was placed in a coolant bath containing acetone and dry ice (●). A cold finger with same was used to condense gaseous ammonia. Once set up anhydrous ammonia (●) was introduced through a hose (a) until the linters were submerged. The setup is sealed, allowing one exit for escaping gas (b).

2.1 Ammonia Treatment

Liquid anhydrous ammonia at atmospheric pressure was used in a closed system (Figure 1) to treat the cotton linters. The ammonia (R717, AGA) was kept liquid by use of a bath of dry-ice in acetone. After 8 hours submerged in ammonia, the reaction vessel was opened and removed from the coolant bath. The opened reaction vessel was allowed to reach room temperature, and the ammonia was allowed to evaporate overnight. The following day, the treated linters were submerged in deionized water and boiled for 6 hours. This boiling was performed to revert the allomorph from cellulose III to cellulose I (Figure 2).

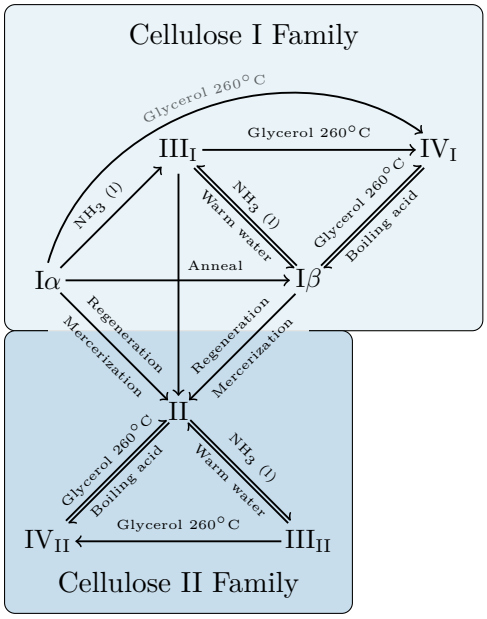

Fig. 2 Crystal allomorphs in cellulose and common pathways for conversion between these. (Kroon-Batenburg et al. 1996; Park et al. 2003; Perez and Mazeau 2005; Zugenmaier 2008; Dufresne 2012; Lavoine et al. 2012).

Once boiled, the linters were dried overnight at 100°C before further treatment. In the case where multiple treatments were conducted (CNF-3), these steps were performed once per treatment. Control samples with no ammonia treatment (CNF-0) were still boiled in DI-water and dried overnight as described.

2.2 Fibrillation

Once any pre-treatment was conducted, fibrillation was performed. Fibrillation was a three-step process; first the linters were beaten in a PFI-mill for 10,000 revolutions at 10% solids. After beating, the linters were ground by running them through a Masuko brand supermasscolloider 10 times at approximately 1% solids. After grinding, they were run through a Rannie 15 type 12.56x homogenizer 5 times at slightly below 1% solids. The first pass through the homogenizer was run at 600 bar pressure drop. All subsequent passes were run at 1 kbar pressure drop.

2.3 Characterization of CNF

Fibrillated material was run through a L&W FiberTester Plus+, assessing the degree of fibrillation by optical means. 5 beakers containing 1 g dry matter suspended in 300 mL DI-water were analyzed for each of the three assessed treatments (CNF-0, CNF-1 and CNF-3). FiberTester Plus+ results were compared with laser profilometry investigation of finished films. Fibrils were further investigated by atomic force microscopy (AFM). AFM samples were prepared by drop casting of 0.02 wt% CNF suspension, on freshly cleaved mica discs (F7013 Agar Scientific) and dried by heating on a 65°C hotplate. Fibril diameter was ascertained by measuring the fibril height above the mica surface, avoiding overestimation due to tip-sample convolution, expected to be large due to the tip radius of the used tips, Bruker ScanAsyst Fluid, which have a nominal tip radius of 20 nm and a maximal radius 60 nm. Areas chosen for diameter estimation were chosen if judged to be a sufficient distance from points where fibrils meet, cross or split/merge. This was done to maximize the likelihood that the measured fibrils are in close contact with the underlying mica, as opposed to suspended above it. A Veeco Multimode V AFM was used in Veeco's software assisted tapping mode named ScanAsyst. Oscillation parameters were controlled by the software. Tips used were ScanAsyst Fluid, whether the image was taken in air or liquid. Samples were first imaged in air, the tip was withdrawn and deionized water was added. After 30 minutes of submersion, the tip was engaged again, and a new image was recorded. AFM micrograph analysis was performed using Gwyddion v. 2.42 (Nečas and Klapetek 2012). AFM micrographs were flattened/leveled using median of differences row alignment, and profiles used for fibril diameter measurements were created using linear interpolation and 10 pixel wide measurement lines spanning one fibril each. Images used for measurements were 1024 by 1024 pixel

large, with 11.7 nm/pixel within the plane of the micrograph. The instrument manufacturer (Veeco) reports a z-noise below 30 pm RMS for the diMultimode V AFM used in the current work. The instrument is located in a cleanroom environment (ISO 7), where it is placed on a vibration dampened table positioned on a reinforced concrete plinth, which is separate from the main floor of the lab to reduce vibrations. Scales in z-direction are indicated by look-up-table (LUT) for each recorded image. For shown visual representations, a 256 value (0-255) gray-scale LUT is applied.

2.3.1 NMR and WAXS - Structural Changes and Crystallinity Measurements

Crystallinity was assessed using two techniques which will be described individually below. The used techniques were Cross-Polarization Magic Angle Spinning Carbon-13 Nuclear Magnetic Resonance (CP/MAS ^{13}C-NMR) - here referred to as NMR - and Wide Angle X-Ray Scattering (WAXS). NMR results were also used to estimate lateral fibril dimension (LFD), lateral fibril aggregate dimension (LFAD) and LFAD specific surface area (LFAD SSA).

CP/MAS ^{13}C-NMR spectra were recorded in a Bruker Avance III AQS 400 SB instrument operating at 9.4 T. All samples were packed uniformly in a zirconium oxide rotor. All measurements were carried out at 295 ($\pm$1) K with a magic angle spinning (MAS) rate of 10 kHz. A 4 mm double air-bearing probe was used. Data acquisition was performed using a cross-polarization (CP) pulse sequence, i.e., a 2.95 microseconds proton 90-degree pulse and an 800 microseconds ramped (100-50%) falling contact pulse, with a 2.5 s delay between repetitions. A SPINAL64 pulse sequence was used for 1H decoupling. The Hartmann-Hahn matching procedure was based on glycine. The chemical shift scale was calibrated to the TMS-scale (tetramethylsilane, $(CH_3)_4Si$) by assigning the data point of maximum intensity in the alpha-glycine carbonyl signal to a shift of 176.03 ppm. 4096 transients were recorded on each sample leading to an acquisition time of about 3 h. The software for spectral fitting was developed at Innventia AB and is based on a Levenberg-Marquardt algorithm (P. T. Larsson et al. 1997). All computations were based on integrated signal intensities obtained from spectral fitting (Wickholm et al. 1998). The errors given for parameters obtained from the fitting procedure are the standard error of the mean with respect to the quality of the fit.

When used to estimate LFD, LFAD and LFAD SSA, the calculations were performed as described in Nocanda et al. 2007. Briefly, Nocanda et al. uses known peak intensities from the signal as a basis for the estimate. The estimate, which relies on further processing, can be expressed thus;

$$q_{LFD} = \frac{I_A + I_I}{\sum I_x} \tag{1}$$

$$q_{LFAD} = \frac{I_A}{\sum I_x}, \tag{2}$$

subscripts for q denote which metric it can be used to estimate. I_x is a given peak intensity for the allomorphs present in the sample, which is assumed to be cellulose I_α and I_β as well as a peak for paracrystalline signal and surface signals for accessible (I_A) and inaccessible (I_I) surfaces. The resulting qs can be used to estimate the dimensions as distances given a known fibril cross-sectional geometry and known glucan dimensions (Nocanda et al. 2007; Wickholm et al. 1998). Nocanda et al. assumed a square cross-section, which means $q = \frac{4n-4}{n^2}$ where n is the number of glucan chains along one side of said cross-section. Knowing the dimensions of a glucan chain cross-section LFD and LFAD can be estimated by solving for n. Equations from Nocanda et al. 2007, where the topic is further discussed.

WAXS measurements were performed on an Anton Paar SAXSpoint 2.0 system (Anton Paar, Graz, Austria) equipped with a Microsource x-ray source (Cu Kα radiation, wavelength 0.15418 nm) and a Dectris 2D CMOS Eiger R 1M detector with 75 µm by 75 µm pixel size. All measurements were performed with a beam size of approximately 500 µm diameter, at a sample stage temperature between 25°C to 29°C (no temperature control was employed) with a beam path pressure at about 1-2 mBar. The sample to detector distance (SDD) was 111 mm. All samples were mounted on a Solid Sampler (Anton Paar, Graz, Austria) mounted on a VarioStage (Anton Paar, Graz, Austria). The samples were exposed to vacuum during measurement. For each sample 5 frames each of 17 minutes duration were read from the detector, giving a total measurement time of 1.4 hour per sample. For all samples the relative transmission was determined and used for scaling of the scattering intensities. The software used for instrument control was SAXSdrive version 2.01.224 (Anton Paar, Graz, Austria), and post-acquisition data processing was performed using the software SAXSanalysis version 3.00.042 (Anton Paar, Graz, Austria). The crystalline index (CI) was estimated from WAXS, in transmission mode, using the Segal method (Segal et al. 1959), where

$$\mathrm{CI} = \frac{I_{200} - I_{am}}{I_{200}} \times 100. \tag{3}$$

Here I_{200} is the intensity of the (200) peak and I_{am} is the amorphous signal at 2θ=18°. The (200) peak was identified using data from untreated samples (CNF-0).

2.4 Production of Films

CNF films were made by solvent casting in plastic petri dishes. CNF suspension with a concentration of 0.85 wt% was poured into the petri dishes and allowed to dry in room temperature. Target grammage was 22 g/m^2. Once dried, the films were conditioned according to ISO 187:1900 prior to characterization.

2.5 Characterization of Films

Films were tensile tested using a Zwick/Roell at 23°C, 50% RH. Specimens were 15 mm wide, the clamp-to-clamp gap was 20 mm. 40 tensile tests were run per sample group (0, 1 or 3 treatments). Tensile indexes of the CNF films were calculated from the average basis weight and average thicknesses of the films. Film thickness was measured by micrometer. The thickness of a given film is assumed to be the average of five measurements on said film. Young modulus was estimated using the point of maximum slope. Yield point was found using an offset of 0.2%. Films were imaged using a Nikon D80 with an HB-47 lens. Electron microscopy (SEM) was employed for high resolution imaging. The electron microscope used was a Hitachi SU4400. Micrographs were recorded using an Everhart-Thornley detector set to collect secondary electrons. Acceleration voltage was set to 5 kV, beam current at 138 µA. All investigated samples were sputter coated with a layer of approximately 12 nm gold prior to SEM analysis. Images were analyzed using FIJI (Schindelin et al. 2012).

2.5.1 Laser Profilometry

From each series, samples of 20 by 10 mm were prepared for laser profilometry (LP). The samples were placed on double-sided tape on microscopy slides and were coated with a layer of gold. 20 laser profilometry (Lehmann, Lehman Mess-Systeme AG, Baden-Dättwil, Germany) topography images were acquired from each sample. The size of the local areas was 1 mm by 1 mm, having a lateral and z-resolution of 1 µm and 10 nm, respectively.

3 Results and Discussion

The current paper discusses the effects of reduced CNF DoC on mechanical properties of CNF films. Treatment by liquid anhydrous ammonia was chosen as the means to reduce DoC because ammonia treatment is known to reduce the DoC of the treated cellulose while maintaining the chemistry and minimally affecting the degree of polymerization (Hess and Trogus 1935; Barry et al. 1936; Rousselle et al. 1976; Saapan et al. 1984; Mittal et al. 2011; Sawada et al. 2014).

The reduced DoC following ammonia treatment is a consequence of the swelling of cellulose by ammonia. Ammonia swells cellulose very well, even penetrating into crystalline areas. When cellulose is swollen with ammonia, hydrogen bonds between cellulose chains are broken, and a nitrogen bridge is established in their place (Wada et al. 2006). This results in a conformational change on a molecular scale - a complex is formed where ammonia molecules are placed between individual cellulose chains. Ammonia can be removed from this complex by evaporation or washing. Inter-chain hydrogen bonds will reform once ammonia is gone, but the unit cell is altered from the original

cellulose I (or II) to a less dense, metastable allomorph named cellulose III_x where $_x$ is either I or II, indicating the allomorph before conversion to cellulose III (Figure 2). The transition from cellulose I to cellulose III_I is, when conducted at atmospheric pressures, also accompanied by a powerful reduction in DoC. How much DoC is affected depends on treatment time (Menachem and Roldan 1971). Reversion to the original allomorph, here cellulose I, is possible by hydrothermal treatment, viz. submersion of cellulose III_I in hot water. This hydrothermal treatment has been reported to increase the DoC somewhat as a function of temperature and treatment time (Menachem and Roldan 1971; Park et al. 2003). Given these aspects of treatment of cellulose with liquid anhydrous ammonia, such a treatment followed by hydrothermal treatment was chosen to investigate the effects of DoC on CNF film properties, fibril properties and degree of fibrillation after homogenization.

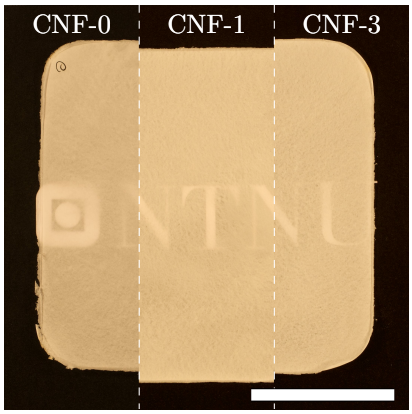

Fig. 3 Images of CNF films, ammonia-treated and controls. Linters received no ammonia treatments (left), one treatment (middle) or three treatments (right). Scale bar is 5 cm long.

Ammonia treatment swells fibrils and films both on a molecular scale and on a macro-scale, resulting in pronounced shrinkage of cellulose based materials once the ammonia is evaporated (Hermann 1997; Thao Ho et al. 2013). In contrast, no immediately apparent difference between untreated and treated CNF can be seen (Figure 3). This is to be expected as the cotton linters were ammonia-treated before fibrillation and film formation. Any macro-scale shrinkage of the produced CNF films can therefore obviously not occur.

3.1 Effects on Crystallinity and Crystal Structure

To assess the change in DoC a wide range of techniques can be employed (Foster et al. 2018; Zugenmaier 2008), two of the experimental techniques that can be used are CP/MAS ^{13}C-NMR, in brief referred to as NMR, and WAXS respectively. For both NMR and WAXS analysis of the materials we see a peak broadening and shift in relative peak intensities correlating with ammonia treatments (Figure 4). This change in the recorded NMR spectra and WAXS profiles is consistent with a reduction in crystalline index.

Analysis of data from the two experimental techniques (NMR, WAXS) supports the initial observations and quantitatively describes the reduction in DoC (Figure 5).

While a clear effect of ammonia treatment on DoC is seen, a stronger response may conceivably be possible if shorter - or no - hydrothermal treatment

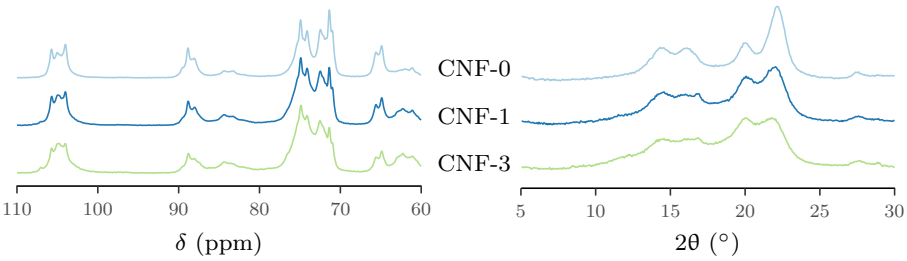

Fig. 4 ^{13}C NMR (left) spectra and WAXS (right) profiles from samples, as annotated. The plots are not normalized. DoC values are shown in Figure 5.

is used. Park et al. 2003 reported higher temperatures or longer submersions in warm water reverses some of the loss of DoC caused by treatment with anhydrous ammonia. We also note that successive treatments with ammonia do have a compounding effect - successive treatments can lower DoC further than a single one. While a compounding effect is seen, there are diminishing returns - the first treatment has the strongest effect.

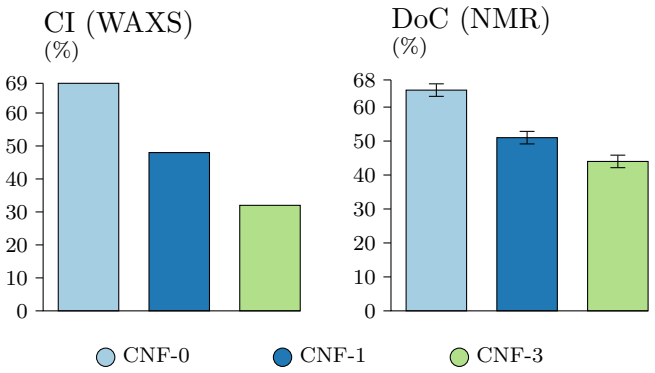

Fig. 5 Crystalline index (CI) from WAXS and degree of crystallinity (DoC) from NMR data. CI was estimated using the Segal method. DoC was calculated using spectral fitting based on Levenberg-Marquardt algorithm. Where error bars are supplied, these indicate standard error of the mean (SE). Cotton linter is nearly pure cellulose, and is assumed to be pure for the purposes of this work.

3.1.1 The presence of cellulose II

From NMR data (Figure 4), in particular a peak at 107 ppm, a small quantity of cellulose II appears present in CNF-1 and CNF-3. The same peak is absent in CNF-0, revealing no cellulose II. The 107 peak, associated with C1 in cellulose II, is fairly well separated from peaks in cellulose I spectra, making

it a good identifier for the allomorph. Most other peaks identifying the allomorph, such as at 105 ppm (C1) 76.5 ppm (C3) and 62.6 and 63 ppm (C6) are present but due to more signal overlap these are less easily detected (Kono and Numata 2004; Zugenmaier 2008). The cellulose II signal is nevertheless small and only resolvable on NMR. In the event that any cellulose II is present in the current experiment, its presence may have resulted from the ammonia swelling step. Cellulose II is commonly a result of dissolution and redispersion of cellulose. When cellulose re-organizes from a dissolved state, the polymeric strands change from the parallel organization in cellulose I to a more thermodynamically stable, anti-parallel configuration - cellulose II. Cellulose II can also be generated by swelling in concentrated alkali, here due to some cellulose chains moving from one fibril to another, adjacent fibril during swelling (Okano and Sarko 1985; Dinand et al. 2002). Cellulose II may be formed by a similar process during swelling with ammonia; polymer chains moving from one fibril to another during swelling may be the cause of the observed cellulose II. Further work is necessary to explore this hypothesis.

3.2 Mechanical Effects of Crystallinity Reduction

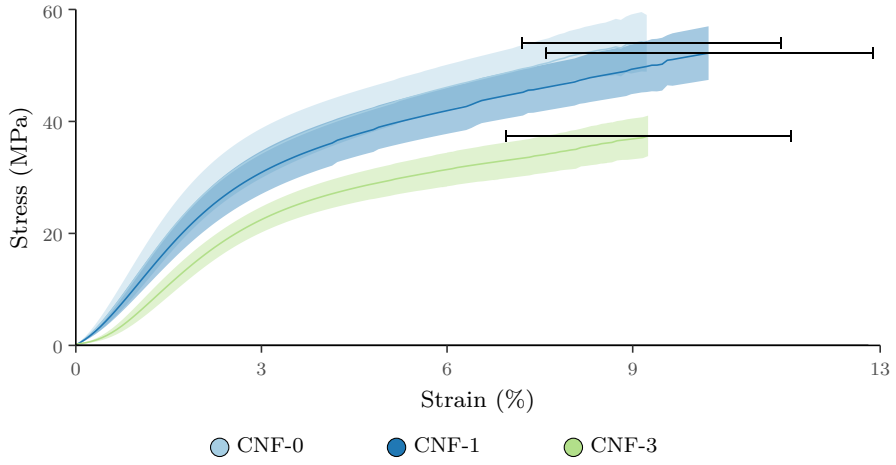

Fig. 6 Stress-Strain curves for tested samples. Colors denote number of ammonia treatments, 0, 1 or 3 as indicated. Ribbons show standard deviation, lines show mean values. For each curves $n = 40$. Lines and ribbons terminate at the mean strain at break, error bars denote standard deviation for strain at break. Strain at break, Young modulus and yield strain are shown in Figure 7. Statistical analysis is shown in Table 1.

As DoC falls, flexibility should increase. In simulations, reduced DoC is shown to weaken fibrils (Youssefian and Rahbar 2015). Increased free volume, which can result from reduction of DoC, has been shown to decrease the Young modulus of the fibrils themselves (Youssefian, Jakes, et al. 2017). As the fibrils

become more flexible, this should be reflected in the properties of produced films. Stress/strain curves (Figure 6) show that there are differing mechanical properties which correlate with DoC. We can note that successive treatments appear to have cumulative effects on the maximum slope of the curves, indicating a reduced Young modulus. Note that Young modulus is estimated as the point of maximum slope. There is a strong correlation between several mechanical properties for the tested films and DoC. This correlation is consistent with the hypothesis that nanofibril DoC has an effect on mechanical properties of films made from them.

While Young modulus and yield point are significantly affected, we cannot conclude strain at break is affected. There is only a barely statistically significant (p=0.047) effect on strain at break between samples CNF-0 and CNF-1 (Table 1). The effect is slight, and not consistent (Figure 7). Hence samples appear equally stretchable, and we cannot conclude there has been an effect.

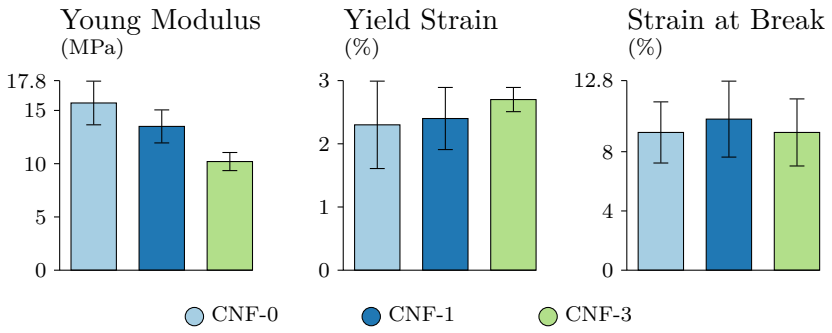

Fig. 7 Plotted values for Young modulus, yield strain and strain at break for tested samples. For each run $n = 40$. Yield strain is defined at 0.2% strain. Young modulus is approximated using the point of maximum slope. Scope and error bars defined by standard deviation. FiberTester Plus+ recorded between 17 059 and 20 027 fibers per run, five runs were completed for each CNF class. Comparisons between group and statistical analysis in Table 1.

As shown in Figure 7 and accompanying statistical analysis in Table 1, we see there is significant differences between treated and untreated samples. Treated and untreated samples differ on both Young modulus (as approximated by the maximal slope of the stress-strain curves) and yield stress (defined at 0.2%). From graph (Figure 7) and accompanying statistical analysis (Table 1), we can conclude that successive ammonia treatments do increase the strain a film can experience before deformation becomes plastic (yield point), and decrease its stiffness (Young modulus) significantly. These observations correlate with change in DoC.

Table 1 Statistical analysis of mechanical properties of ammonia-treated cellulose. Mechanical differences between CNF from cotton linters treated 0, 1 and 3 times were analyzed. Similarly, untreated CNF films were compared with ammonia-treated CNF films. The statistical test used was a Mann-Whitney test, given that upon inspection of the data distribution, normality can not be assumed. For each run $n = 40$. Leftmost column indicates which groups were compared.

	Young modulus		**Yield point**		**Strain at break**	
	p-value	**W**	**p-value**	**W**	**p-value**	**W**
CNF-0-CNF-1	2.6×10^{-8}	1347	0.017	551	0.047	593
CNF-0-CNF-3	$< 2.2 \times 10^{-16}$	1558	4.61×10^{-8}	212.5	0.95	807
CNF-1-CNF-3	$< 2.2 \times 10^{-16}$	1544	2.56×10^{-7}	264	0.060	996

3.3 Structural Differences - for Films and Fibrils

DoC can be seen to correlate with, likely causally, certain mechanical properties of resulting films. It is prudent to ask if the same process might also affect fibrillation and microtopography of the films. Fibril strength is expected to decline as DoC declines (Youssefian and Rahbar 2015), which might increase fibrillation. Several techniques have been employed to ascertain what, if any, effects the ammonia treatment has had on degree of fibrillation. The approaches used have spanned from resolving large features (Profilometry, FiberTester Plus+) to resolving small features (SEM, AFM, NMR).

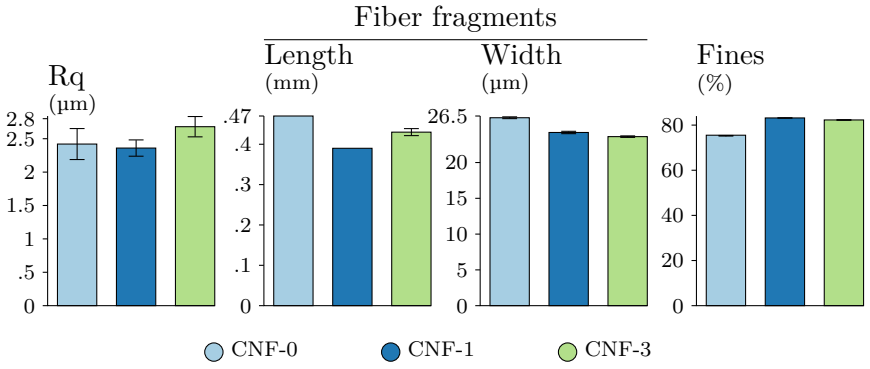

Fig. 8 Metrics pertaining to surface roughness parameter (Rq) obtained by laser profilometry and FiberTester Plus+ results. Scope and error bars defined by standard deviation.

Larger features in pulp or CNF suspensions were quantitatively assessed in suspension (using FiberTester Plus+) as well as using dried films (using laser profilometry). Profilometry can be used as an indirect measure of degree of fibrillation, as smaller fibrils will yield smoother surfaces than larger, less fibrillated samples (Chinga-Carrasco et al. 2008). FiberTester Plus+ uses a camera to conduct measurements of fiber suspensions to measure fiber fragment and fine size distributions among other metrics. Results from FiberTester+ and

profilometry (Figure 8) do not show consistent correlations with DoC, suggesting fibrillation - and fibril morphology - was not affected by ammonia treatments.

SEM (Figures 9) and AFM (figures 9 and 11) also show few tangible differences between samples, further supporting the conclusion that ammonia treatment has not affected fibrillation.

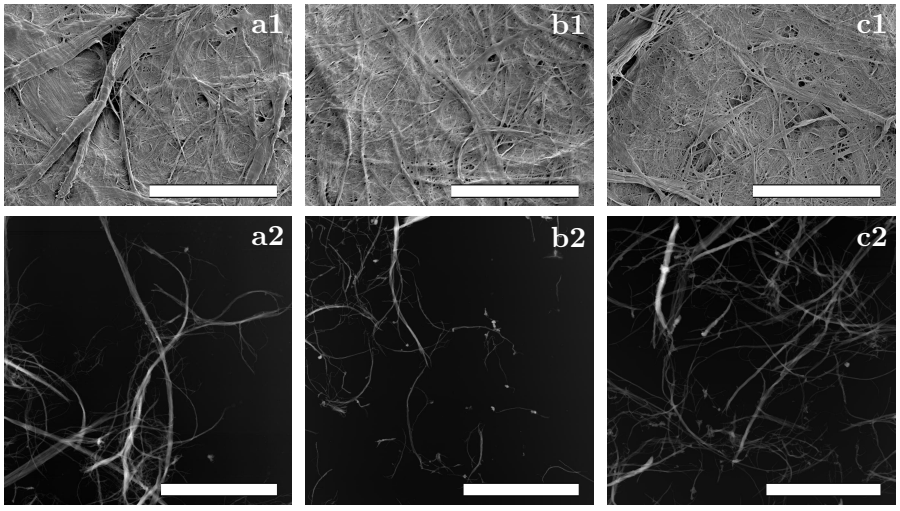

Fig. 9 SEM micrographs of films and AFM micrographs of fibrils. SEM micrographs show CNF-0 (a1, a2), CNF-1 (b1, b2) and CNF-3 (c1, c2). SEM micrographs are numbered 1 and AFM micrographs are numbered 2. SEM scale bars are 40 µm long. AFM micrographs show scale bars 5 µm long. AFM micrographs show height data. AFM LUT goes from black to white, where black represents 0 nm and white represents 159 (a2), 118 (b2) or 252 (c2). AFM micrographs are recorded in air.

NMR is another technique which can assess fibril dimensions. LFAD and LFAD SSA (Wickholm et al. 1998; Hult et al. 2001; Šturcova et al. 2004) (See equation 2 and Figure 10) are measures of available surface area on the fibrils as they would be seen in a microscope. This metric, which shows no large differences between samples and largely overlapping standard errors, further suggests strong morphological similarities between the samples. In other words, NMR results further support the hypothesis that ammonia treatment does not affect fibrillation.

The third metric provided, LFD, includes contribution from *inaccessible* surface area, viz. fibril surfaces within aggregates. As we can see from Figure 10 LFD is strongly affected by ammonia treatment, even though the fibril aggregates appear not to be. This reduction in lateral fibril dimensions is consistent with the appearance of cellulose II in ammonia treated samples; if cellulose II is present and formed by polymer chains leaving one fibril and attaching to another, existing fibril - or joining to form new structures with the cellulose

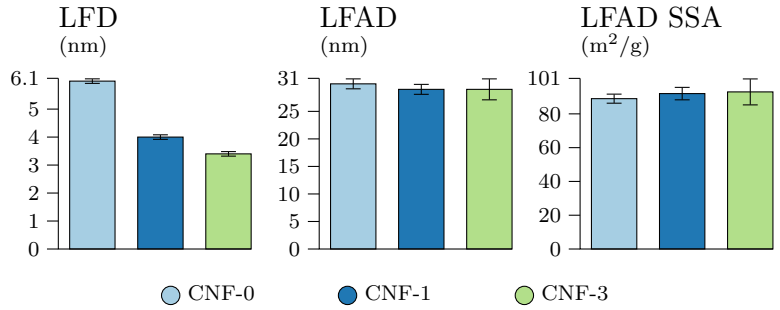

Fig. 10 Lateral fibril dimension (LFD), lateral fibril aggregate dimension (LFAD) and LFAD specific surface area (LFAD SSA) as calculated from ^{13}C NMR (Segal et al. 1959; P. T. Larsson et al. 1997; Wickholm et al. 1998; Hult et al. 2001; Peciulyte et al. 2015). A detailed account for the calculations used is previously reported by Nocanda et al. (Nocanda et al. 2007). Where error bars are supplied, these indicate standard error of the mean (SE).

II allomorph - fibril, if not fibril aggregate, cross-sectional dimensions can be expected to be reduced.

3.4 Fibril Properties- Swelling

AFM as a microscopy technique allows for very high precision measurements of micro to nano-scopic materials. The technique has the added benefit of being usable in atmosphere as well as on samples submerged in liquid. Using this technique, acquisition of the micrographs of the same area while dry and submerged (Figure 11) allows for measurement of fibril diameters in dry and wet state, allowing for measurement of swelling of individual fibrils. It has long been held that swelling can and does occur on a fibril level (Stone and Scallan 1968) while Wang et al. (2012) have shown similar results for fibers of bacterial cellulose during enzymatic degradation, direct measurements for nano-fibrils in dry state as compared with submerged in water is currently absent from the literature.

By measuring fibril diameters on 38 separate locations in dry and swelled state, we were able to measure the swelling of dried CNF, as shown in Figure 12. The mean and median swelling are 48.9 and 48.6% respectively, with a standard deviation of 27.8%. As these fibrils have been dried, it is possible some loss of swell-ability has occurred and that the results do not reflect the state of the elementary fibrils in the cell wall. In the event that swell-ability has been lost, we note that the swelling is still measurable, which probably has consequences for the properties of films produced from the material upon introduction of moisture or change in relative humidity. Given that the increase in diameter measured is not constant, but changes from fibril to fibril, we believe we are measuring swelling and not merely a layer of water molecules tightly associated with the fibril surface. Likely areas for swelling may include regions of the fibril where the degree of crystallinity is low, or less ordered / more

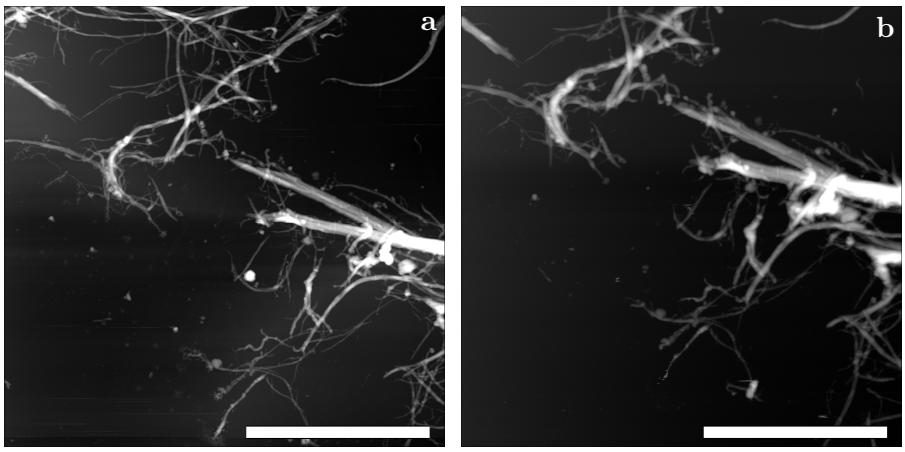

Fig. 11 AFM micrographs of ammonia-treated CNF in air (a) and water (b). Scale bars are 5 µm long. The LUT goes from zero (black) to white, which is at 186.4 (a) and 195.5 nm (b) respectively. Both images show fibrillated linters from CNF-3.

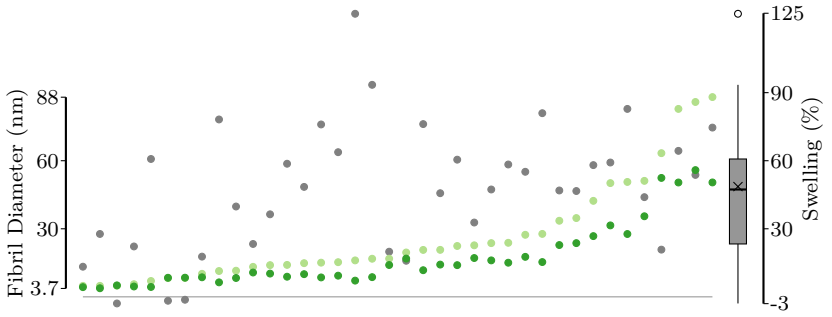

Fig. 12 Fibril diameters from Figure 11. Measurements are from 38 individual points in air (●) and water (●), respectively. Swelling, in %, is also shown in the same plot (●) and as a boxplot by the rightmost axis. The horizontal line across the plot shows a swelling of 0% and a fibril diameter of 0 nm respectively. y-scales are limited to the range of the presented data. Measurements sorted according to fibril diameter measured in water. The points aligned vertically are from the same point on the same fibril in both air and water. The box plot shows mean (horizontal line) and median (×). An outlier is shown above the box plot as a hollow circle.

amorphous. In disordered regions it seems likely water molecules are more likely to enter a given fibril and swell it. For bundles of elementary fibrils, the area between these may also serve as a likely candidate for swelling. Given that cotton linters are nearly pure cellulose, the swelled material is unlikely to be other components of the source plant, e.g. hemicellulose. As crystallinity is reduced, e.g. by ammonia treatment, it seems possible swell-ability of nanofibrils may be increased. As CNF from CNF-3 was used for the above measurements, the swelling may be higher than for most CNF qualities due to the sample's reduced degree of crystallinity. Further work can shed light on the role of DoC in swelling.

4 Conclusions

The degree of crystallinity (DoC) of cotton linters was reduced while retaining a predominantly cellulose I allomorph by submersion in liquid anhydrous ammonia and subsequent boiling in de-ionized (DI)-water.

Our main conclusion based on the work presented herein is that the degree of crystallinity does affect mechanical properties; reduced degree of crystallinity (DoC) correlates with increased elastic domain (increased yield point) as well as reduced Young-modulus. In summary:

1. The crystallinity of the sample was reduced by the used ammonia treatment scheme. The first ammonia treatment had the most effect; subsequent treatments had less effect on DoC and CI. Crystallinity was primarily reported as DoC measured using ^{13}C NMR, though crystalline index (CI), measured using WAXS, was also supplied.
2. A small amount of cellulose II is seen in the ammonia treated samples. This is slight, below WAXS detection limit. We hypothesize this is due to some few cellulose polymer chains being removed from their host fibrils during ammonia treatment, reforming in an anti-parallel fashion, giving rise to cellulose II.
3. DoC was seen to correlate with Young modulus. The effect was notable, and highly significant.
4. DoC was seen to have an inverse correlation with yield point. The effect was slight, but statistically significant.
5. DoC is not shown to affect strain at break; no correlation was found for strain at break.
6. Ammonia treatment was seen to alter the internal structure of the fibril aggregates, increasing inaccessible surface areas, reducing LFD. A similar effect on fibril aggregates (LFAD) was not seen.
7. Ammonia treatment was not seen to affect degree of fibrillation, which was assessed using profilometry, FiberTester +, AFM, SEM and NMR.

Using AFM to examine CNF-3 in air and water we were also able to demonstrate swelling of individual CNFs (fibrils and fibril aggregates) upon submersion in DI water. From the range of fibril diameters measured (3.7 to 88 nm), swelling appears to affect nano-fibers with a wide range of diameters. This result demonstrates that swelling of dry cellulose materials is not relegated to the fiber or network size range, but also occurs on a nano-fibril level.

Acknowledgements This work is performed as a part of the NORCEL Project: The NORwegian NanoCELlulose Technology Platform, initiated and led by The Paper and Fiber Research Institute (PFI) in Trondheim and funded by the Research Council of Norway through the NANO2021 Program (grant 228147 Research Council of Norway). The Research Council of Norway is further acknowledged for the support to the Norwegian Micro- and Nano-Fabrication Facility, NorFab. Thanks are extended to CELSUR for providing cotton linters. Thanks are further extended to Jasna Stevanic Srndovic for assistance with NMR and WAXS measurements, Kelly McCammon-Ottesen for proof-reading.

References

Aulin, Christian, Mikael Gällstedt, and Tom Lindström (Jan. 2010). "Oxygen and oil barrier properties of microfibrillated cellulose films and coatings". In: *Cellulose* 17.3, pp. 559–574. ISSN: 0969-0239. DOI: 10.1007/s10570-009-9393-y.

Barry, A. J., F. C. Peterson, and A. J. King (Feb. 1936). "x-Ray Studies of Reactions of Cellulose in Non-Aqueous Systems. I. Interaction of Cellulose and Liquid Ammonia 1". In: *J. Am. Chem. Soc.* 58.2, pp. 333–337. ISSN: 0002-7863. DOI: 10.1021/ja01293a043.

Brodin, Malin et al. (Sept. 2017). "Lignocellulosics as sustainable resources for production of bioplastics – A review". In: *J. Clean. Prod.* 162, pp. 646–664. ISSN: 09596526. DOI: 10.1016/j.jclepro.2017.05.209.

Chinga-Carrasco, G. et al. (2008). "New advances in the 3D characterization of mineral coating layers on paper". In: *J. Microsc.* 232.2, pp. 212–224. ISSN: 00222720. DOI: 10.1111/j.1365-2818.2008.02092.x.

Codou, Amadine et al. (2015). "Partial periodate oxidation and thermal cross-linking for the processing ofthermosetall-cellulose composites". In: *Compos. Sci. Technol.* 117, pp. 54–61. DOI: 10.1016/j.compscitech.2015.05.022.

Dinand, Elizabeth et al. (2002). "Mercerization of primary wall cellulose and its implication for the conversion of cellulose I → cellulose II". In: *Cellulose* 9.1, pp. 7–18. ISSN: 09690239. DOI: 10.1023/A:1015877021688.

Dufresne, Alain (2012). *Nanocellulose: From Nature to High Performance Tailored Materials*. Walter de Gruyter. ISBN: 3110254603.

Foster, E Johan et al. (2018). *Current characterization methods for cellulose nanomaterials*. DOI: 10.1039/c6cs00895j.

Fukuzumi, Hayaka et al. (Jan. 2009). "Transparent and High Gas Barrier Films of Cellulose Nanofibers Prepared by TEMPO-Mediated Oxidation". In: *Biomacromolecules* 10.1, pp. 162–165. ISSN: 1525-7797. DOI: 10.1021/bm801065u.

Ginestet, Cedric (2011). "ggplot2: Elegant Graphics for Data Analysis". In: *J. R. Stat. Soc. Ser. A (Statistics Soc.* 174.1, pp. 245–246. ISSN: 0006341X. DOI: 10.1111/j.1541-0420.2011.01616.x.

Henriksson, Marielle et al. (June 2008). "Cellulose Nanopaper Structures of High Toughness". In: *Biomacromolecules* 9.6, pp. 1579–1585. ISSN: 1525-7797. DOI: 10.1021/bm800038n.

Hermann, Christine K. F. (Nov. 1997). "The shrinking dollar bill". In: *J. Chem. Educ.* 74.11, p. 1357. ISSN: 0021-9584. DOI: 10.1021/ed074p1357.2.

Hess, K. and C. Trogus (1935). "Über Ammoniak-Cellulose (Vorläuf. Mitteil.)" In: *Berichte der Dtsch. Chem. Gesellschaft (A B Ser.* 68.10, pp. 1986–1988. ISSN: 03659488. DOI: 10.1002/cber.19350681016.

Hult, Eva L., Per T. Larsson, and Tommy Iversen (2001). "Cellulose fibril aggregation - An inherent property of kraft pulps". In: *Polymer (Guildf).* 42.8, pp. 3309–3314. ISSN: 00323861. DOI: 10.1016/S0032-3861(00)00774-6.

Kono, Hiroyuki and Yukari Numata (June 2004). "Two-dimensional spin-exchange solid-state NMR study of the crystal structure of cellulose II". In:

572 *Polymer (Guildf).* 45.13, pp. 4541–4547. ISSN: 00323861. DOI: 10.1016/j.
573 polymer.2004.04.025.
574 Kroon-Batenburg, L M J, B Bouma, and J Kroon (1996). "Stability of Cel-
575 lulose Structures Studied by MD Simulations. Could Mercerized Cellulose
576 II Be Parallel?" In: *Macromolecules* 29.17, pp. 5695–5699. ISSN: 0024-9297.
577 DOI: 10.1021/ma9518058.
578 Kumar, Vinay et al. (June 2016). "Influence of nanolatex addition on cellulose
579 nanofiber film properties". In: *Nord. Pulp Pap. Res. J.* 31.02, pp. 333–340.
580 ISSN: 0283-2631. DOI: 10.3183/NPPRJ-2016-31-02-p333-340.
581 Larsson, Per A, Lars A Berglund, and Lars Wågberg (June 2014). "Ductile all-
582 cellulose nanocomposite films fabricated from core-shell structured cellu-
583 lose nanofibrils." In: *Biomacromolecules* 15.6, pp. 2218–23. ISSN: 1526-4602.
584 DOI: 10.1021/bm500360c.
585 Larsson, Per A and Lars Wågberg (2016). "Towards natural-fibre-based ther-
586 moplastic films produced by conventional papermaking". In: *Green Chem.*
587 18.11, pp. 3324–3333. DOI: 10.1039/c5gc03068d.
588 Larsson, Per Tomas, Kristina Wickholm, and Tommy Iversen (July 1997). "A
589 CP/MAS13C NMR investigation of molecular ordering in celluloses". In:
590 *Carbohydr. Res.* 302.1-2, pp. 19–25. ISSN: 00086215. DOI: 10.1016/S0008-
591 6215(97)00130-4.
592 Lavoine, Nathalie et al. (Oct. 2012). "Microfibrillated cellulose - its barrier
593 properties and applications in cellulosic materials: a review." In: *Carbohydr.*
594 *Polym.* 90.2, pp. 735–64. ISSN: 1879-1344. DOI: 10.1016/j.carbpol.2012.
595 05.026.
596 Menachem, Lewin and Luis G. Roldan (1971). "the Effect of Liquid Anhy-
597 drous Ammonia in the structure and morphology of cotton cellulose". In:
598 *J. Polym. Sci. Part C Polym. Symp.* 229.36, pp. 213–229.
599 Minelli, Matteo et al. (Aug. 2010). "Investigation of mass transport properties
600 of microfibrillated cellulose (MFC) films". In: *J. Memb. Sci.* 358.1-2, pp. 67–
601 75. ISSN: 03767388. DOI: 10.1016/j.memsci.2010.04.030.
602 Mittal, Ashutosh et al. (Jan. 2011). "Effects of alkaline or liquid-ammonia
603 treatment on crystalline cellulose: changes in crystalline structure and ef-
604 fects on enzymatic digestibility". In: *Biotechnol. Biofuels* 4.41, pp. 1–16.
605 ISSN: 1754-6834. DOI: 10.1186/1754-6834-4-41.
606 Myllytie, Petri et al. (2010). "Viscoelasticity and water plasticization of polymer-
607 cellulose composite films and paper sheets". In: *Cellulose* 17.2, pp. 375–385.
608 ISSN: 09690239. DOI: 10.1007/s10570-009-9376-z.
609 Nečas, David and Petr Klapetek (Jan. 2012). "Gwyddion: an open-source soft-
610 ware for SPM data analysis". In: *Open Phys.* 10.1. ISSN: 2391-5471. DOI:
611 10.2478/s11534-011-0096-2.
612 Nishino, Takashi, Ikuyo Matsuda, and Koichi Hirao (2004). "All-Cellulose
613 Composite". In: *Macromolecules* 37.20, pp. 7683–7687. ISSN: 00249297. DOI:
614 10.1021/ma049300h.
615 Nocanda, Xolani et al. (Jan. 2007). "Cross polarisation/magic angle spinning
616 13C-NMR spectroscopic studies of cellulose structural changes in hard-

wood dissolving pulp process". In: *Holzforschung* 61.6, pp. 675–679. ISSN: 1437434X. DOI: 10.1515/HF.2007.095.

Nogi, Masaya et al. (Apr. 2009). "Optically Transparent Nanofiber Paper". In: *Adv. Mater.* 21.16, pp. 1595–1598. ISSN: 09359648. DOI: 10.1002/adma.200803174.

Okano, Takeshi and Anatole Sarko (Jan. 1985). "Mercerization of cellulose. II. Alkali–cellulose intermediates and a possible mercerization mechanism". In: *J. Appl. Polym. Sci.* 30.1, pp. 325–332. ISSN: 00218995. DOI: 10.1002/app.1985.070300128.

Park, Sun-Ji et al. (2003). "Effect of Dry Heat and Hot Water Processings on Cellulose III Crystallite of Cotton and Lyocell Fibers Treated with Liquid Ammonia." In: *Sen'i Gakkaishi* 58.8, pp. 299–303. ISSN: 0037-9875. DOI: 10.2115/fiber.58.299.

Peciulyte, Ausra et al. (Dec. 2015). "Impact of the supramolecular structure of cellulose on the efficiency of enzymatic hydrolysis". In: *Biotechnol. Biofuels* 8.56, pp. 1–13. ISSN: 1754-6834. DOI: 10.1186/s13068-015-0236-9.

Perez, Serge and and Karim Mazeau (2005). "Conformations, Structures, and Morphologies of Celluloses". In: *Polysaccharides Struct. Divers. Funct. Versatility*, pp. 41–68. DOI: 10.1201/9781420030822.ch2.

R Core Team (2015). *R: A Language and Environment for Statistical Computing*. DOI: 10.1017/CBO9781107415324.004.

Rodionova, Galina et al. (Feb. 2012). "Mechanical and oxygen barrier properties of films prepared from fibrillated dispersions of TEMPO-oxidized Norway spruce and Eucalyptus pulps". In: *Cellulose* 19.3, pp. 705–711. ISSN: 0969-0239. DOI: 10.1007/s10570-012-9664-x.

Rousselle, Marie A. et al. (Apr. 1976). "Liquid-ammonia And Caustic Mercerization Of Cotton Fibers: Changes In Fine Structure And Mechanical Properties". In: *Text. Res. J.* 46.4, pp. 304–310. ISSN: 00405175. DOI: 10.1177/004051757604600412.

Saapan, A.A., Sherif H. Kandil, and Abdel M. Habib (Dec. 1984). "Liquid Ammonia and Caustic Mercerization of Cotton Fibers Using X-Ray, Infrared, and Sorption Measurements". In: *Text. Res. J.* 54.12, pp. 863–867. ISSN: 0040-5175. DOI: 10.1177/004051758405401212.

Sawada, Daisuke et al. (Mar. 2014). "The initial structure of cellulose during ammonia pretreatment". In: *Cellulose* 21.3, pp. 1117–1126. ISSN: 0969-0239. DOI: 10.1007/s10570-014-0218-2.

Schindelin, Johannes et al. (July 2012). "Fiji: an open-source platform for biological-image analysis." In: *Nat. Methods* 9.7, pp. 676–82. ISSN: 1548-7105. DOI: 10.1038/nmeth.2019.

Segal, Leon et al. (1959). "An Empirical Method for Estimating the Degree of Crystallinity of Native Cellulose Using the X-Ray Diffractometer". In: *Text. Res. J.* 29.10, pp. 786–794. ISSN: 0040-5175. DOI: 10.1177/004051755902901003.

Stone, J. E. and A. M. Scallan (1968). "A Structural Model for the Cell Wall of Water Swollen Wood Fibres Based on Their Accessibility to Macromolecules". In: *Cellul. Chem. Technol.* 2, pp. 343–358.

Šturcova, Adriana et al. (2004). "Structural details of crystalline cellulose from higher plants". In: *Biomacromolecules*. ISSN: 15257797. DOI: 10.1021/bm034517p.

Syverud, Kristin and Per Stenius (Aug. 2008). "Strength and barrier properties of MFC films". In: *Cellulose* 16.1, pp. 75–85. ISSN: 0969-0239. DOI: 10.1007/s10570-008-9244-2.

Thao Ho, Thi Thu et al. (Apr. 2013). "Liquid ammonia treatment of (cationic) nanofibrillated cellulose/vermiculite composites". In: *J. Polym. Sci. Part B Polym. Phys.* 51.8, pp. 638–648. ISSN: 08876266. DOI: 10.1002/polb.23241.

Wada, Masahisa, Yoshiharu Nishiyama, and Paul Langan (Apr. 2006). "X-ray Structure of Ammonia-Cellulose I: New Insights into the Conversion of Cellulose I to Cellulose III I". In: *Macromolecules* 39.8, pp. 2947–2952. ISSN: 0024-9297. DOI: 10.1021/ma060228s.

Wang, Jingpeng et al. (2012). "Real-time observation of the swelling and hydrolysis of a single crystalline cellulose fiber catalyzed by cellulase 7B from Trichoderma reesei". In: *Langmuir* 28.25, pp. 9664–9672. ISSN: 07437463. DOI: 10.1021/la301030f.

Wickholm, Kristina, Per Tomas Larsson, and Tommy Iversen (1998). "Assignment of non-crystalline forms in cellulose I by CP/MAS 13C NMR spectroscopy". In: *Carbohydr. Res.* 312.3, pp. 123–129. ISSN: 00086215. DOI: 10.1016/S0008-6215(98)00236-5.

Youssefian, Sina, Joseph E. Jakes, and Nima Rahbar (2017). "Variation of Nanostructures, Molecular Interactions, and Anisotropic Elastic Moduli of Lignocellulosic Cell Walls with Moisture". In: *Sci. Rep.* 7.1, pp. 1–10. ISSN: 20452322. DOI: 10.1038/s41598-017-02288-w.

Youssefian, Sina and Nima Rahbar (2015). "Molecular origin of strength and stiffness in bamboo fibrils". In: *Sci. Rep.* 5, pp. 1–13. ISSN: 20452322. DOI: 10.1038/srep11116.

Zugenmaier, Peter (2008). *Crystalline cellulose and cellulose derivatives*. Springer. ISBN: 9783540739333.